Liquid Crystals
Publication details, including instructions for authors and subscription information:
http://www.informaworld.com/smpp/title~content=t713926090

Crystal structures of ferro- and antiferroelectric mesogens with a 1-methylalkoxycarbonyl group

Kayako Hori[a]; Sumie Kawahara[a]
[a] Department of Chemistry, Ochanomizu University, Tokyo, Japan

To cite this Article Hori, Kayako and Kawahara, Sumie(1996) 'Crystal structures of ferro- and antiferroelectric mesogens with a 1-methylalkoxycarbonyl group', Liquid Crystals, 20: 3, 311 — 319
To link to this Article: DOI: 10.1080/02678299608032040
URL: http://dx.doi.org/10.1080/02678299608032040

LIQUID CRYSTALS, 1996, VOL. 20, NO. 3, 311–319

Crystal structures of ferro- and antiferroelectric mesogens with a 1-methylalkoxycarbonyl group

by KAYAKO HORI* and SUMIE KAWAHARA
Department of Chemistry, Ochanomizu University, Otsuka, Bunkyo-ku, Tokyo 112, Japan

(*Received 26 July 1995; accepted 6 October 1995*)

Crystal structures have been determined for 4-[(*S*)-1-methylpentyloxycarbonyl]phenyl, 4-([*S*)-1-methylhexyloxycarbonyl]phenyl 4′-octyloxybiphenyl-4-carboxylates (**1** and **2**, respectively) and (*R*)-1-methylheptyl 4-(4′-octyloxybiphenyl-4-yloxymethylene)benzoate (**3**), which have $S^*_{C_A}$, S^*_C and $S^*_{C_A}$ phases, respectively. All the crystals have a common packing mode with the previously determined structure of 4-(1-methylheptyloxycarbonyl)phenyl 4′-octyloxybiphenyl-4-carboxylate (MHPOBC). Each crystal forms a smectic-like layer structure composed of largely bent molecules with the long alkyl chain of the chiral group almost perpendicular to the core moiety. Differential scanning calorimetry showed that the crystals of **1**, **2**, and MHPOBC, which have a carbonyloxy group as the central linkage between the biphenyl and phenylene moieties, transform to higher temperature solid phases in a similar temperature range (around 60°C). For **3**, which has an oxymethylene linkage between the biphenyl and phenylene moieties, three kinds of solids were distinguished.

1. Introduction

Since the discovery of antiferroelectric liquid crystalline phases for 4-(1-methylheptyloxycarbonyl)phenyl 4′-octyloxybiphenyl-4-carboxylate (MHPOBC) [1], a number of antiferroelectric mesogens have been synthesized. For example, a homologous series of MHPOBC, in which the length of the longer chain of the chiral group varies, show the S^*_C and/or $S^*_{C_A}$ phase, depending on the chain length; $S^*_{C_A}$ for $n = 3$ and 4, S^*_C for $n = 5$ [2], and $S^*_{C_A}$ and S^*_C for $n = 6$ [1].

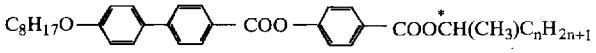

We have found some correlation between crystal structures and liquid crystalline phase sequences for several series of chiral biphenyl esters [3]. Thus, we carried out single crystal X-ray analysis also for the compounds with $n = 4$ (**1**) and 5 (**2**). As reported briefly [4], however, both crystal structures are very similar to that of a metastable but frequently encountered form of MHPOBC [5]; almost perpendicularly bent molecules are packed in a smectic-like layer structure. This is probably because energy difference between the ferro- and antiferroelectric phases is very small as was confirmed by a calorimetric study [6]. However, the fact that almost the same structure is found regardless of the chain length suggests that such a bent structure is characteristic to chiral 1-methylalkoxycarbonyl groups.

*Author for correspondence.

Therefore, we extended X-ray structure analysis to other compounds with a chiral 1-methylalkoxycarbonyl group. The following substances, in which the carbonyloxy group between the biphenyl and phenylene groups of MHPOBC is substituted by an oxymethylene or a methyleneoxy group, also have the $S^*_{C_A}$ phase [7].

1-methylheptyl 4-(4′-octyloxybiphenyl-4-yloxymethylene)benzoate (**3**)

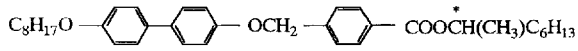

Cr85(S_{X_2} 83·0)S_{X_1} 106·5S_I 120·0$S^*_{C_A}$ 132·0S^*_C 133·5°C

1-methylheptyl 4-(4′-octyloxybiphenyl-4-ylmethyleneoxy)benzoate (**4**)

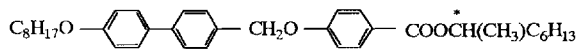

Cr78(S_X 72·8)$S^*_{C_A}$ 94·2S^*_C 100·1S_A 108·0°C

Here, it is noteworthy that the phase sequences are quite different according to the direction of the central linkage group. Especially, the former substance transforms to the isotropic phase without passing through S_A, in contrast to most compounds with $S^*_{C_A}$ which show S_A.

This paper describes the crystal structures of (*S*)-forms of **1** and **2** and the (*R*)-form of **3** and the thermal

0267–8292/96 $12·00

behaviour of the crystal structures to their higher temperature phases. For **4**, the data collected were insufficient for crystal structure determination with large overall temperature factor (Wilson's $B > 6$) even at $-50°C$.

2. Experimental

2.1. *Compounds*

The compounds **1** and **2** were supplied by Mitsubishi Gas Chemical Ltd., **3** and **4** supplied by Chisso Petrochemical Corp. Single crystals were obtained by slow evaporation from a solution of diethyl ether/methanol (for **1**), diethyl ether/1-butanol (for **2**), ethyl acetate/1-butanol (for **3**) and ethyl acetate/methanol (for **4**).

2.2. *Apparatus*

DSC measurements were done on a Seiko DSC22C. Powder X-ray diffraction patterns were obtained on a Rigaku RAD-RA diffractometer.

2.3. *X-ray crystal structure analysis*

Cell parameter measurements and reflection data collection were done on an AFC-7R four-circle diffractometer using CuK_α radiation monochromated by graphite ($\lambda = 1{\cdot}54184$ Å) at room temperature for **1–3.** For **4**, the data were collected at room temperature and $-50°C$. Both data sets were insufficient for structure analysis partly due to the small size of the crystal in spite of repeated attempts at crystallization and partly due to the large overall temperature factor B (8·2 at RT and 6·5 at $-50°C$). The 2θ-ω mode (except for **2,** to which ω mode was applied because peak profiles were broad with shoulders) was applied with scan rates of $8° min^{-1}$ (ω) (for **1–3**) and 2 and $4° min^{-1}$ (ω) (for **4**, at RT and $-50°C$, respectively) up to $2\theta = 120°$. Three standard reflections were measured after every 150 reflections. No significant variation was observed. All the data were corrected for Lorentz and polarization factors. Detailed experimental conditions and crystal data are summarized in table 1.

All the structures were solved by applying the teXsan program package [8] and refined by the full-matrix least-squares method on F^2 by using SHELXL93 [9]. Each benzene ring was constrained to have a regular hexagonal geometry with C–C distances of 1·39 Å and were refined as a rigid group. Slightly restrained condition was applied to several bonds of alkyl chains. In crystal **3**, terminal atoms C(37) and C(38) in the chiral group had a remarkably large temperature factors and small peaks were found around them. Therefore,

Table 1. Experimental details, crystal data, and final results of refinements.

Parameter	**1**	**2**	**3**
Formula	$C_{34}H_{42}O_5$	$C_{35}H_{44}O_5$	$C_{36}H_{48}O_4$
Formula weight	530·68	544·70	544·74
Crystal habit	needle	long plate	long plate
Crystal size/mm	0·3 × 0·1 × 0·1	0·4 × 0·2 × 0·1	0·6 × 0·6 × 0·02
X-ray source	CuK_α (1·54184 Å)		
Monochrometer	graphite		
Diffractometer	AFC-7R		
L.s. for cell const.[a]	17($39 < 2\theta < 55°$)	16($42 < 2\theta < 49°$)	25($48 < 2\theta < 50°$)
Crystal system	monoclinic	monoclinic	monoclinic
Space group	$P2_1$	$P2_1$	$P2_1$
a/Å	29·943(3)	31·251(5)	33·132(3)
b/Å	5·486(3)	5·482(6)	5·512(5)
c/Å	9·376(5)	9·393(8)	9·069(5)
β/°	95·18(2)	98·86(3)	95·49(2)
V/Å^3	1533·8(12)	1590(2)	1649(2)
Z	2	2	2
d_x/Mg m^{-3}	1·149	1·139	1·097
μ/mm^{-1}	0·600	0·591	0·544
$F(000)$	572	588	592
No. of unique reflections	2550	2625	2724
No. of reflections ($>4\sigma(F_o)$)	1403	1397	1691
S	0·931	0·948	1·043
R_1[b]	0·070	0·071	0·094
R_{w2}[c]	0·224	0·208	0·278

[a] No. of reflections with the 2θ range in parentheses.
[b] $R_1 = \Sigma ||F_o| - |F_c|| / \Sigma |F_o|$ for observed reflections.
[c] $R_{w2} = [\Sigma w(F_o^2 - F_c^2)^2 / \Sigma w(F_o^2)^2]^{0.5}$ for observed reflections, where $w = [\sigma^2(F_o^2) + \{a(F_o^2 + 2F_c^2)/3\}^2]^{-1}$ ($a = 0{\cdot}2409$, 0·1556, and 0·2203 for **1**, **2**, and **3**, respectively).

these atoms were disordered in further refinement. Temperature factors for some of the disordered atoms still became large, which were fixed. All the non-hydrogen atoms except for the disordered atoms were refined anisotropically. Hydrogen atoms calculated geometrically (C–H distances; 0·96 (for primary), 0·97 (for secondary), 0·98 (for tertiary) and 0·93 Å (for aromatic)) for the anisotropically refined C atoms were included in the intensity calculation but not refined. Final results of refinements are also summarized in table 1. R factors based on F^2 were about three times larger than those based on F for all the crystals, slightly larger than those statistically expected to be about twice as large. Scattering factors were taken from the International Tables for Crystallography [10]. Final atomic coordinates are shown in tables 2–4.

3. Results and discussion

3.1. *Molecular structure*

Figure 1 shows the molecular structures of **1**, **2** and **3** with numbering schemes. All the molecules have almost the same conformation. First, biphenyl moieties are coplanar with dihedral angles of 2·2(9) (**1**), 1·6(13) (**2**), and 1·1(11)° (**3**). Second, all the long chains have all-*trans* conformations except for the disordered moiety in **3**. Third, the long chain of the chiral group is almost perpendicular to the molecular long axis. These features are also observed in one of the crystalline polymorphs of MHPOBC [5]. The C(31)–O(4) bond length is slightly longer than the expected value, 1·43 Å, in **1** (1·482(9) Å) and **2** (1·491(8) Å). All other bond lengths and angles are normal within experimental errors.

3.2. *Crystal packing*

Figures 2–4 show the crystal structures of **1–3** viewed along the b axis. It is shown that all the crystals have almost the same packing mode. Bent-shaped molecules are packed alternately, forming a smectic-like layer structure. The layer interfaces are parallel to the (1 0 0) plane. The moiety, except for the chain of a chiral group, takes an anti-parallel arrangement along the c axis and contributes to a large overlapping of the molecules within a layer, while the chains of the chiral groups face each other between adjacent layers. Thus, the structures have alternate stacking of chiral chain moieties and remaining parts. 'Partial' densities are estimated to be 0·78–0·79 and 1·23–1·28 g cm^{-3} for the former and the latter, respectively, for all the crystals. However, the large difference in the densities is due to the difference in weights of contents, especially the ratios of hydrogen atoms included in the two parts. The volume per atom (including both non-hydrogen and hydrogen atoms), which could be regarded as a rough measure of packing efficiency, was found to be almost the same, i.e.

Table 2. Atomic coordinates and equivalent isotropic displacement parameters for **1**.

Atom	x	y	z	U_{eq}[a]/Å^2
O(1)	0·6295(2)	0·3745(16)	1·0162(6)	0·078(2)
O(2)	0·3342(2)	0·3137(16)	0·3024(6)	0·074(2)
O(3)	0·3164(2)	0·6576(19)	0·4136(6)	0·094(2)
O(4)	0·1406(2)	0·1422(19)	−0·0056(7)	0·089(2)
O(5)	0·1566(2)	0·500(2)	−0·1075(8)	0·114(3)
C(1)	0·5885(1)	0·3944(15)	0·9395(5)	0·063(2)
C(2)	0·5783(2)	0·2129(15)	0·8383(6)	0·081(3)
C(3)	0·5379(2)	0·2196(15)	0·7530(5)	0·075(2)
C(4)	0·5076(1)	0·4077(16)	0·7689(5)	0·058(2)
C(5)	0·5178(2)	0·5892(15)	0·8701(6)	0·081(3)
C(6)	0·5582(2)	0·5826(15)	0·9554(5)	0·076(2)
C(7)	0·4635(1)	0·4212(15)	0·6720(5)	0·058(2)
C(8)	0·4534(2)	0·2501(15)	0·5645(6)	0·070(2)
C(9)	0·4139(2)	0·2702(15)	0·4753(5)	0·074(2)
C(10)	0·3845(1)	0·4614(16)	0·4936(5)	0·062(2)
C(11)	0·3946(2)	0·6325(15)	0·6010(6)	0·086(3)
C(12)	0·4341(2)	0·6124(15)	0·6902(5)	0·086(3)
C(13)	0·3418(3)	0·490(2)	0·4029(8)	0·071(2)
C(14)	0·2939(1)	0·3160(16)	0·2167(6)	0·071(2)
C(15)	0·2829(2)	0·5039(16)	0·1205(6)	0·077(2)
C(16)	0·2415(2)	0·5042(15)	0·0402(5)	0·078(2)
C(17)	0·2112(1)	0·3164(16)	0·0561(6)	0·071(2)
C(18)	0·2222(2)	0·1284(15)	0·1523(6)	0·078(2)
C(19)	0·2636(2)	0·1282(15)	0·2326(6)	0·076(2)
C(20)	0·1676(3)	0·324(2)	−0·0285(10)	0·081(3)
C(21)	0·6440(3)	0·567(2)	1·1097(9)	0·078(3)
C(22)	0·6907(3)	0·517(2)	1·1740(9)	0·079(2)
C(23)	0·7085(3)	0·718(2)	1·2724(10)	0·088(3)
C(24)	0·7557(3)	0·686(3)	1·3352(10)	0·096(3)
C(25)	0·7738(4)	0·918(3)	1·4173(12)	0·123(4)
C(26)	0·8205(4)	0·899(3)	1·4868(16)	0·157(7)
C(27)	0·8276(6)	1·133(4)	1·5766(19)	0·199(9)
C(28)	0·8744(7)	1·137(7)	1·643(3)	0·303(16)
C(31)	0·0961(3)	0·135(3)	−0·0887(10)	0·098(3)
C(32)	0·1025(4)	0·009(4)	−0·2316(11)	0·137(5)
C(33)	0·0669(3)	−0·005(3)	−0·0005(12)	0·111(4)
C(34)	0·0579(4)	0·116(3)	0·1365(13)	0·119(4)
C(35)	0·0228(5)	−0·020(4)	0·2171(15)	0·159(6)
C(36)	0·0156(6)	0·118(6)	0·3558(18)	0·221(10)

[a] U_{eq} is defined as one third of the trace of the orthogonalized U_{ij} tensor.

9·6 Å^3 for the chiral chain moiety and 9·4 Å^3 for the remaining part. The volume per methylene group is estimated to be 29(= 9·6 × 3) Å^3, which is larger than those obtained for crystalline long-chain compounds, 23–25 Å^3 [12], and even that estimated for the liquid state, 27 Å^3 [13]. Therefore, the chains are found to be loosely packed between layers.

Tilt angles of the molecular long axes are estimated to be about 30° in all the crystals. However, the relative orientation of the molecular long axis to the unit cell is different between the former two (along the [2 0 $\bar{1}$] axis) and **3** (along the [2 0 1] axis). The direction of the latter is the same as that of MHPOBC, in accordance with

Table 3. Atomic coordinates and equivalent isotropic displacement parameters for **2**.

Atom	x	y	z	U_{eq}[a]/Å^2
O(1)	0·1255(1)	0·8266(13)	0·0412(5)	0·091(2)
O(2)	−0·1597(1)	0·7678(13)	−0·7324(5)	0·088(1)
O(3)	−0·1782(2)	1·1081(16)	−0·6221(5)	0·113(2)
O(4)	−0·3461(2)	0·5977(17)	−1·0764(6)	0·114(2)
O(5)	−0·3314(2)	0·9429(17)	−1·1787(7)	0·140(2)
C(1)	0·0856(1)	0·8483(14)	−0·0417(4)	0·076(2)
C(2)	0·0566(2)	1·0371(13)	−0·0312(4)	0·087(2)
C(3)	0·0174(1)	1·0449(13)	−0·1239(5)	0·093(2)
C(4)	0·0073(1)	0·8639(14)	−0·2272(4)	0·070(2)
C(5)	0·0363(1)	0·6751(13)	−0·2378(4)	0·085(2)
C(6)	0·0755(1)	0·6672(13)	−0·1450(5)	0·094(2)
C(7)	−0·0351(1)	0·8760(13)	−0·3354(4)	0·068(2)
C(8)	−0·0638(1)	1·0662(13)	−0·3241(4)	0·097(2)
C(9)	−0·1021(1)	1·0832(13)	−0·4210(5)	0·093(2)
C(10)	−0·1117(1)	0·9099(13)	−0·5292(4)	0·074(2)
C(11)	−0·0830(1)	0·7196(13)	−0·5405(4)	0·083(2)
C(12)	−0·0447(1)	0·7027(13)	−0·4437(5)	0·083(2)
C(13)	−0·1526(2)	0·9458(19)	−0·6304(7)	0·083(2)
C(14)	−0·1987(1)	0·7704(14)	−0·8244(5)	0·086(2)
C(15)	−0·2277(2)	0·5809(13)	−0·8152(5)	0·090(2)
C(16)	−0·2676(1)	0·5793(13)	−0·9042(5)	0·098(2)
C(17)	−0·2784(1)	0·7673(14)	−1·0025(5)	0·086(2)
C(18)	−0·2494(2)	0·9567(13)	−1·0117(4)	0·094(2)
C(19)	−0·2096(1)	0·9583(13)	−0·9226(5)	0·094(2)
C(20)	−0·3212(3)	0·781(2)	−1·0960(10)	0·097(2)
C(21)	0·1390(2)	1·0200(16)	0·1376(7)	0·084(2)
C(22)	0·1841(2)	0·965(2)	0·2105(7)	0·096(2)
C(23)	0·2009(2)	1·162(2)	0·3170(8)	0·104(3)
C(24)	0·2484(2)	1·132(2)	0·3895(8)	0·109(3)
C(25)	0·2650(3)	1·358(2)	0·4732(9)	0·143(4)
C(26)	0·3097(3)	1·344(3)	0·5546(14)	0·186(6)
C(27)	0·3178(5)	1·588(3)	0·638(2)	0·279(10)
C(28)	0·3590(6)	1·548(6)	0·726(3)	0·380(15)
C(31)	−0·3892(2)	0·582(2)	−1·1685(11)	0·122(3)
C(32)	−0·3864(3)	0·458(3)	−1·3081(9)	0·168(5)
C(33)	−0·4181(3)	0·449(3)	−1·0841(11)	0·144(4)
C(34)	−0·4249(4)	0·576(3)	−0·9430(12)	0·152(4)
C(35)	−0·4594(4)	0·454(3)	−0·8684(14)	0·167(4)
C(36)	−0·4641(4)	0·563(4)	−0·7255(15)	0·201(7)
C(37)	−0·4972(5)	0·426(5)	−0·6567(15)	0·260(9)

[a] U_{eq} is defined as one third of the trace of the orthogonalized U_{ij} tensor.

Table 4. Atomic coordinates and equivalent isotropic displacement parameters for **3**.

Atom	x	y	z	U_{eq}[a]/Å^2 or U_{iso}[b]/Å^2
O(1)	0·3816(2)	0·2094(16)	0·4453(7)	0·075(2)
O(2)	0·6399(2)	0·2357(16)	−0·0117(6)	0·073(2)
O(4)	0·8320(3)	0·039(3)	−0·2936(11)	0·126(3)
O(5)	0·8127(3)	0·400(3)	−0·3838(14)	0·149(4)
C(1)	0·4193(2)	0·2187(16)	0·3937(6)	0·060(2)
C(2)	0·4478(2)	0·4007(15)	0·4274(6)	0·074(3)
C(3)	0·4842(2)	0·3992(15)	0·3629(6)	0·067(2)
C(4)	0·4922(2)	0·2157(16)	0·2647(6)	0·059(2)
C(5)	0·4637(2)	0·0336(15)	0·2310(6)	0·070(2)
C(6)	0·4273(2)	0·0351(15)	0·2954(7)	0·074(3)
C(7)	0·5327(2)	0·2134(16)	0·1917(6)	0·057(2)
C(8)	0·5608(2)	0·3988(15)	0·2201(6)	0·075(3)
C(9)	0·5964(2)	0·3998(16)	0·1500(7)	0·077(3)
C(10)	0·6038(2)	0·2154(16)	0·0516(6)	0·060(2)
C(11)	0·5757(2)	0·0300(15)	0·0232(6)	0·068(2)
C(12)	0·5401(2)	0·0290(15)	0·0933(6)	0·068(2)
C(13)	0·6509(3)	0·030(3)	−0·0992(11)	0·084(3)
C(14)	0·6911(2)	0·0866(19)	−0·1552(8)	0·073(3)
C(15)	0·6976(2)	0·2970(18)	−0·2340(8)	0·092(3)
C(16)	0·7352(2)	0·3393(17)	−0·2853(7)	0·091(3)
C(17)	0·7663(2)	0·1712(19)	−0·2577(8)	0·083(3)
C(18)	0·7598(2)	−0·0392(18)	−0·1789(8)	0·084(3)
C(19)	0·7222(2)	−0·0815(17)	−0·1276(7)	0·090(3)
C(20)	0·8055(4)	0·215(4)	−0·3195(15)	0·105(4)
C(21)	0·3701(3)	0·403(2)	0·5352(10)	0·073(3)
C(22)	0·3269(3)	0·369(2)	0·5664(10)	0·077(3)
C(23)	0·3117(3)	0·590(2)	0·6493(11)	0·080(3)
C(24)	0·2678(4)	0·570(3)	0·6830(11)	0·089(3)
C(25)	0·2536(4)	0·797(3)	0·7550(13)	0·099(4)
C(26)	0·2112(4)	0·793(3)	0·7946(14)	0·107(4)
C(27)	0·1977(6)	1·023(4)	0·863(2)	0·166(8)
C(28)	0·1552(6)	1·030(6)	0·892(3)	0·221(11)
C(31)	0·8708(5)	0·050(5)	−0·351(2)	0·157(7)
C(32)	0·8703(6)	−0·118(6)	−0·484(2)	0·188(10)
C(33)	0·9016(6)	−0·066(8)	−0·241(3)	0·250(19)
C(34)	0·9071(8)	0·028(7)	−0·091(3)	0·232(14)
C(35)	0·9417(6)	−0·077(9)	0·010(3)	0·28(2)
C(36)	0·9441(10)	0·048(11)	0·157(3)	0·31(2)
C(37)	0·9895(14)	0·02(2)	0·196(13)	0·31
C(37′)	0·9852(9)	0·027(9)	0·248(5)	0·235(12)
C(38)	0·981(2)	−0·187(14)	0·304(6)	0·21(2)
C(38′)	0·976(4)	0·23(3)	0·359(14)	0·33
C(38″)	1·002(4)	−0·03(3)	0·409(11)	0·30

[a] U_{eq} is defined as one third of the trace of the orthogonalized U_{ij} tensor.

[b] Isotropic temperature factors U_{iso} was applied to C(37), C(37′), C(38), C(38′), and C(38″), whose occupancies were fixed to be 0·4, 0·6, 0·4, 0·3, and 0·3, respectively. Temperature factors for C(37), C(38′), and C(38″) were fixed.

almost the same molecular dimensions of these two compounds. In addition, terminal atoms of the long chain of the chiral group are disordered in these two crystals. It is considered that the hexyl chain is slightly too long to be packed in the space available between layers.

Figure 5 shows the crystal structures viewed along the c axis. As was found in the crystal of MHPOBC [5], carbonyloxy groups form infinite chains of head-to-tail arrangements along the b axis in all the crystals. The directions of the head-to-tail arrangements for two kinds of carbonyloxy groups are the same in the crystals of **1** or **2**. For **3**, the more electronegative O in C=O than that in C–O–C of a carbonyloxy group and O in an oxymethylene group point upward along the b axis, showing that the b axis components of dipole moments of the two polar groups are in the same direction.

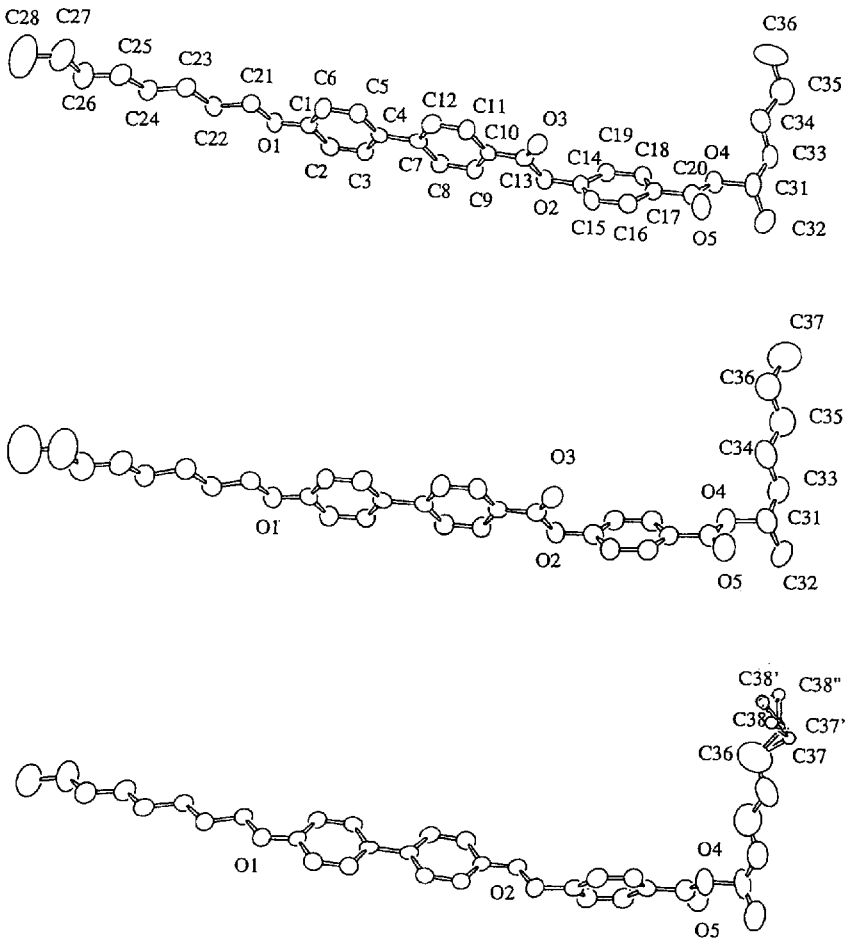

Figure 1. ORTEP drawings [11] of **1** (upper), **2** (middle), and **3** (lower) with 30 per cent probability thermal ellipsoids. In **3**, C37′ is almost hidden by C37.

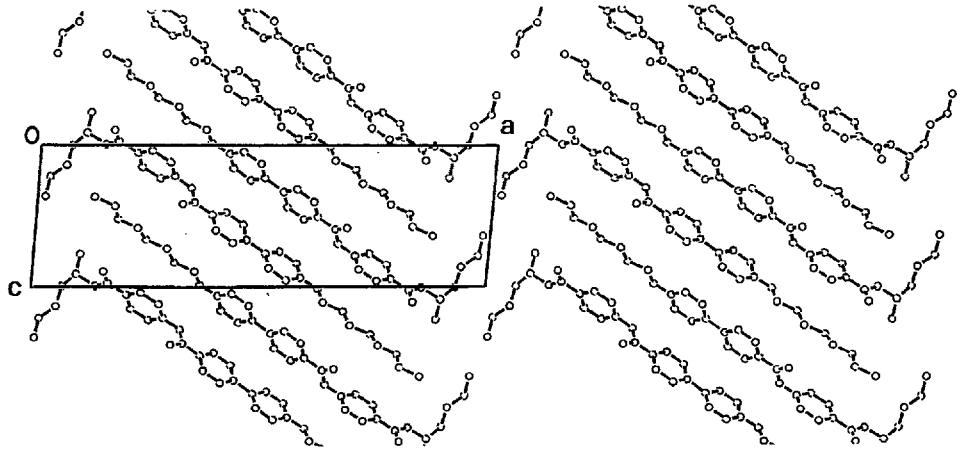

Figure 2. Crystal structure of **1** viewed along the *b* axis.

Therefore, all the components of the dipole moment associated with the polar groups are additive along the *b* axis in all the crystals as in those of MHPOBC. Figure 6 shows the core moieties viewed along the molecular long axis. All the crystals are composed of a pseudo-hexagonal array with an apex angle of about 110°. The angle between adjacent biphenyl moieties are about 65° in all the crystals.

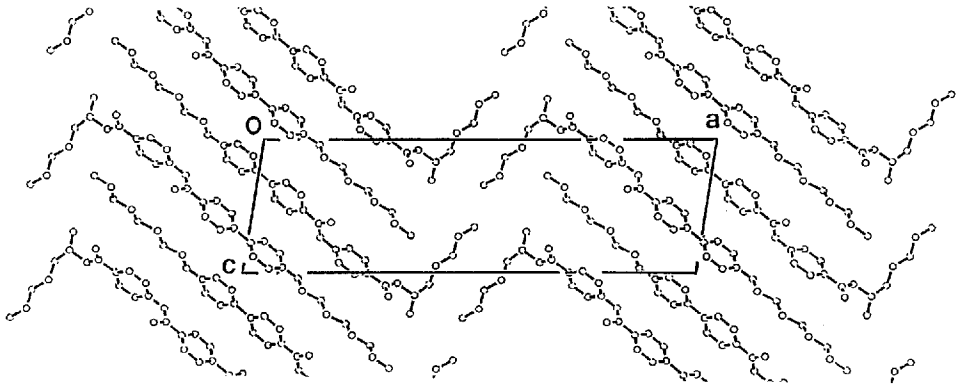

Figure 3. Crystal structure of **2** viewed along the *b* axis.

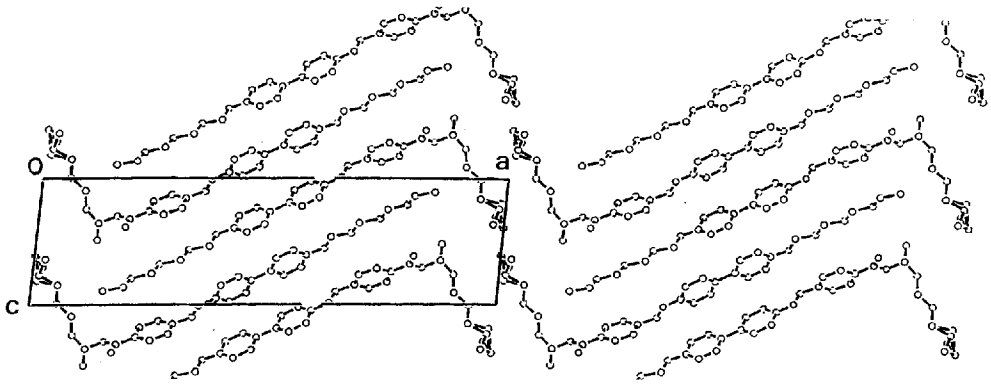

Figure 4. Crystal structure of **3** viewed along the *b* axis.

For **4**, although the structure has not been analysed, the crystal data were obtained as follows. Monoclinic, $a = 35{\cdot}209(10)$, $b = 8{\cdot}153(9)$, $c = 5{\cdot}800(8)$ Å, $\beta = 90{\cdot}37(10)°$, $V = 1665(3)$ Å^3 at room temperature and $a = 35{\cdot}563(10)$, $b = 7{\cdot}948(16)$, $c = 5{\cdot}728(11)$ Å, $\beta = 92{\cdot}85(9)°$, $V = 1617(4)$ Å^3 at -50°C. The unit cell dimension is similar to that of **3**, while the direction of the unique axis is altered. Comparing the data at RT and -50°C, thermal expansion coefficients are obtained to be $1{\cdot}4 \times 10^{-4}$, $3{\cdot}6 \times 10^{-4}$ and $1{\cdot}8 \times 10^{-4}$ K^{-1} along the *a*, *b*, and *c* axes, respectively. It is noteworthy that the coefficient along the *a* axis is negative, suggesting a change in the tilt angle of the molecular long axis relative to the *a* axis or a shrinkage in the length of the molecule caused by thermal disorder, as was discussed for the smectic A [14]. The β value changes significantly. In addition, the overall temperature factor is large even at -50°C, as already mentioned in §2. All these facts suggest that in crystal **4**, thermal motions would play an important role.

3.3. *Thermal behaviour of the crystals*

Figure 7 shows DSC traces on heating for **1**, and **2**. For comparison, a curve for MHPOBC is also shown. The complicated behaviour of MHPOBC was interpreted [5] as the crystal transforms to a higher temperature crystal at the peak (*a*), the higher temperature crystal begins to transform to $S^*_{C_A}$ at the peak (*b*), then triggered by the onset of this transition, immediately stabilizes to a more stable crystalline state at the exothermic peak (*c*), and the stable crystal transforms to $S^*_{C_A}$ again at peak (*d*). A Raman spectral study revealed that peak (*b*) is due to a partial melting of the chains [15]. On the other hand, **1** and **2** show small peaks ((*e*) and (*g*), respectively) associated with solid solid transitions before they transform to their mesophases at the peaks (*f*) (**1**) and (*h*) (**2**). However, neither give exothermic peaks, showing that the present crystals and their higher temperature phases are thermodynamically stable in the temperature range concerned. In spite of the difference of thermodynamical stability, each crystal of **1**, **2**, and MHPOBC, which has a carbonyloxy group between biphenyl and phenylene groups, shows solid–solid phase transition in a similar temperature region before it transforms to S^*_C or $S^*_{C_A}$.

On the contrary, compound **3** shows no thermal anomaly until it transforms to S_X, while the transition behaviour to S_X is rather complicated. DSC traces for

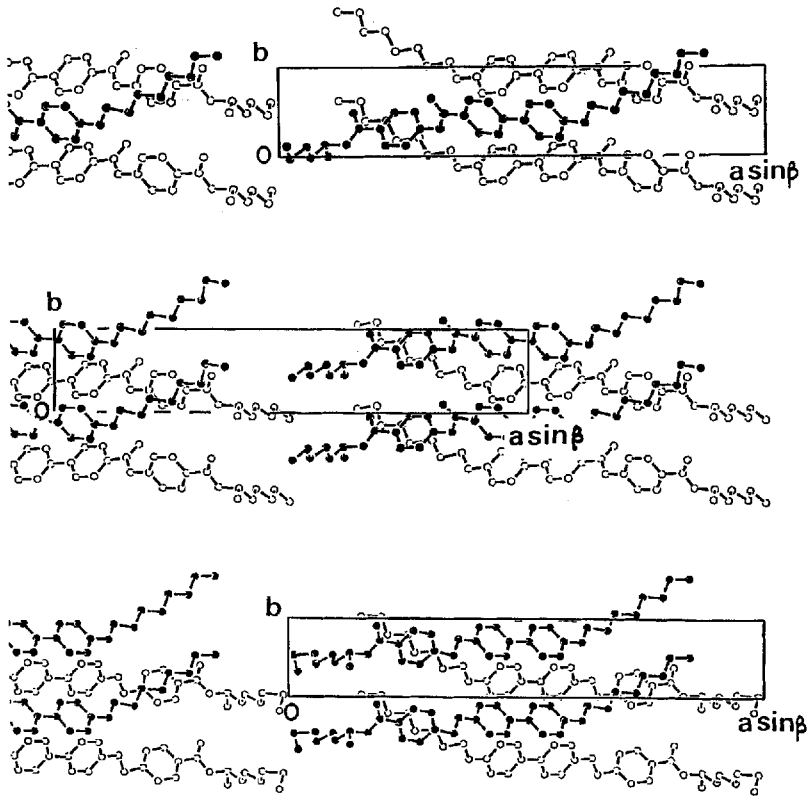

Figure 5. Crystal structures of **1** (upper), **2** (middle), and **3** (lower) viewed along the *c* axis. Atoms of the front molecules are denoted by solid circles. For **3**, disordered atoms are omitted for clarity.

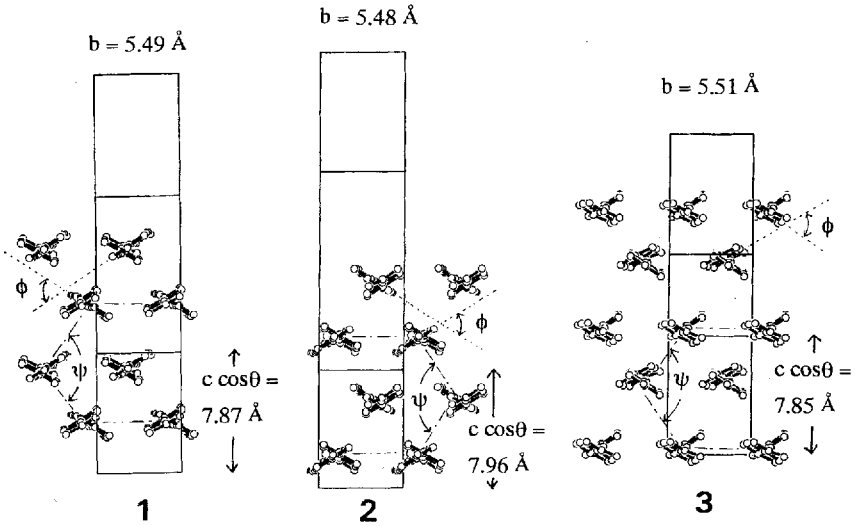

Figure 6. Packing mode of core moieties of **1** (left), **2** (middle), and **3** (right) viewed along the molecular long axis. θ is a tilt angle of the molecular long axis. ϕ made by dotted lines denotes an angle between adjacent biphenyl moieties. ψ made by dot-and-dash lines denotes the apex angle of a hexagon.

long plate single crystals (i), for which the crystal structure has been determined, powder specimen as supplied (ii), and solid obtained from melt (iii) are shown in figure 8. Curve (i) shows a sharp melting peak (*a*) followed by a broad peak (*b*), while the curve (ii) shows only a broad peak (*g*) on melting. The broadness of the latter is not due to the sample purity, because the solid obtained from the melt (iii) showed a sharp peak (*h*) on

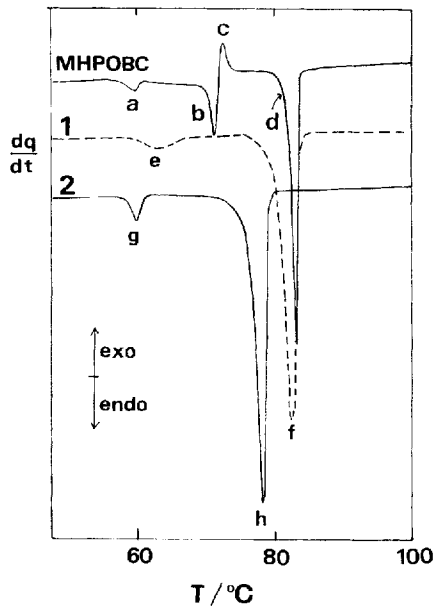

Figure 7. DSC traces on heating with the heating rate of 1 K min^{-1} of **1**, **2**, and MHPOBC. The crystal to a higher temperature crystal (*a*), the higher temperature crystal to $S^*_{C_A}$ (*b*) transitions, stabilization to a more stable crystalline state (*c*), and the stable crystal to $S^*_{C_A}$ transition (*d*) for MHPOBC. The crystal to a higher temperature crystal (*e*) and the higher temperature crystal to $S^*_{C_A}$ (*f*) transitions for **1**. The crystal to a higher temperature crystal (*g*) and the higher temperature crystal to $S^*_{C_A}$ (*h*) transition for **2**.

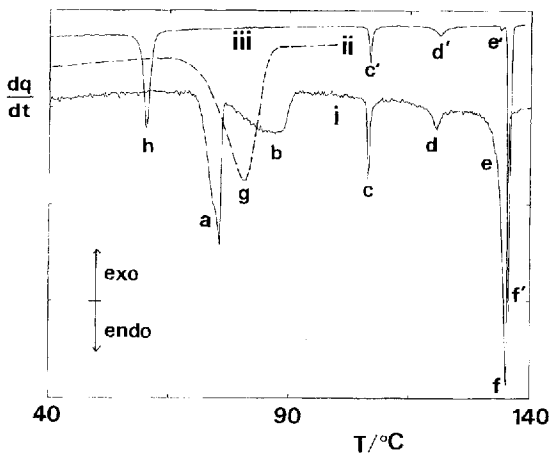

Figure 8. DSC traces on heating with the heating rate of 1 K min^{-1} of **3**; long plate crystals (i), powder specimen as received (ii) and solid obtained from melt of ii (iii). The meltings of the long plate crystal (*a*), the specimen as supplied (*g*), and the sample obtained from the melt (*h*). The transitions from S_X to S^*_I (*c* and *c'*), from S^*_I to $S^*_{C_A}$ (*d* and *d'*), from $S^*_{C_A}$ to S^*_C (*e* and *e'*), and from S^*_C to I (*f* and *f'*). The nature of the peak *b* has not been clarified.

reheating, although the peak position lowered and the ΔH value was about a half of the original ΔH of 24 ± 3 kJ mol^{-1}. Moreover, the position of peak (*g*) for (ii) varied from sample to sample, roughly dependent on the heating rate, for example, 70 ± 5, 76 ± 2 and 82 ± 1°C at the heating rate of 0·5, 2 and 10 K min^{-1}, respectively. These features are rather strange as melting behaviour. The nature of the peak (*g*), as well as that of the peak (*b*), should be further studied by other methods such as time-resolved spectroscopy, which is now in preparation. X-ray diffraction patterns showed that these three kinds of solid have different structures, as shown in figure 9. Here, for the long plate crystal, a simulated pattern of the present crystal structure is shown, because of the very small amount of the crystals.

It is concluded that bent-shape molecules, in which the long chain of the chiral group is almost perpendicular to the core moiety, are frequently found in the crystalline states of chiral mesogens with 1-methylalkoxycarbonyl groups, as long as the chain length fits the space available in the smectic-like layers. It was also found that the structures transform to the higher temperature solid in a similar manner for the compounds with carbonyloxy group as the central linkage of the biphenyl and phenylene moieties. For the compound with an oxymethylene linkage between the biphenyl and phenylene moieties, three kinds of solid were distinguished.

The authors express their thanks to Mitsubishi Gas Chemical Ltd. for supplying compounds **1** and **2**, and to Chisso Petrochemical Corporation for supplying compounds **3** and **4**. This work was supported by a Grant-

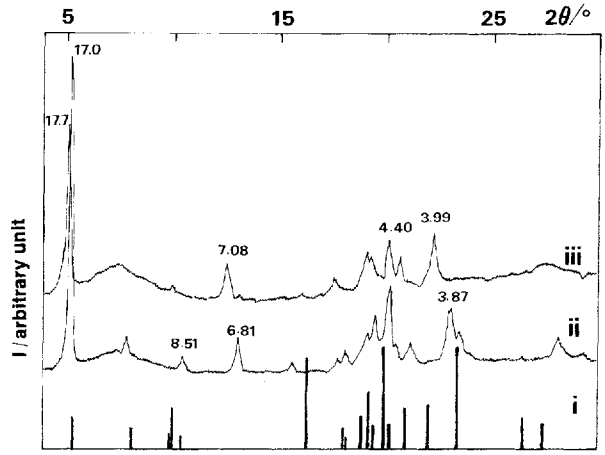

Figure 9. X-ray powder pattern simulated for the present crystal structure by using the program PULVERIX [16] (i), and powder diffraction patterns for powder specimens as received (ii) and solid obtained from melt of ii (iii). In the simulation of i, hydrogen atoms and disordered atoms were omitted. Numerical values given at the peaks are *d* values (Å).

in-Aid from Hayashi Memorial Foundation for Female Natural Scientists to K.H.

References

[1] CHANDANI, A. D. L., OUCHI, Y., TAKEZOE, H., FUKUDA, A., TERASHIMA, K., FURUKAWA, K., and KISHI, A., 1989, *Jpn. J. appl. Phys.*, **28,** L1261.

[2] JOHNO, M., and YUI, T., 1992, *Future Liquid Crystal Displays and its Materials*, edited by A. Fukuda (Tokyo: CMC), Chap. 14 (in Japanese).

[3] ITO, K., ENDO, K., HORI, K., NEMOTO, T., UEKUSA, H., and OHASHI, Y., 1994, *Liq. Cryst.*, **17,** 747 and references cited therein.

[4] HORI, K., KAWAHARA, S., and ITO, K., 1993, *Ferroelectrics*, **147,** 91.

[5] HORI, K., and ENDO, K., 1993, *Bull. chem. Soc. Jpn.*, **66,** 46.

[6] ASAHINA, S., SORAI, M., FUKUDA, A., TAKEZOE, H., FURUKAWA, K., TERASHIMA, K., SUZUKI, Y., and KAWAMURA, I., 1993, *Abstracts of Fourth International Conference of Ferroelectric Liquid Crystals*, 28 September–1 October, Tokyo, Japan, P-35.

[7] NEUNDORF, D., DIELE, S., ERNST, S., SAITO, S., DEMUS, D., INUKAI, T., and MURASHIRO, K., 1993, *Ferroelectrics*, **147,** 95; *Abstracts of Fourth International Conference of Ferroelectric Liquid Crystals*, 28 September–1 October, Tokyo, Japan, P-21.

[8] teXsan, 1985 and 1992, *Crystal Structure Analysis Package*, Molecular Structure Corporation.

[9] SHELDRICK, G. M., 1993, SHELXL93, program for the refinement of the crystal structure, University of Gottingen, Germany.

[10] 1992, *International Tables for Crystallography*, edited by A. J. C. Wilson, Vol. C (Dordrecht: Kluwer Academic Publishers).

[11] JOHNSON, C., 1965, ORTEP, Report ORNL-3794, Oak Ridge National Laboratory, Tennessee, U.S.A.

[12] ABRAHAMSSON, S., 1959, *Ark. Kemi*, **11,** 65.

[13] The volume per methylene unit in the liquid state was estimated as difference in the molar volumes for C_nH_{2n+2} and $C_{n+1}H_{2n+4}$ which were derived from density data at 20°C [*Tables for Oils and Fats*, 1958, edited by the Japan Oil Chemists' Society, (Maruzen, Tokyo), p. 110].

[14] KUMAR, S., 1984, *Phys. Rev. A*, **23,** 3207.

[15] KIM, K. H., TAKANISHI, Y., ISHIKAWA, K., TAKEZOE, H., and FUKUDA, A., 1994, *Liq. Cryst.*, **16,** 185. In this article, they concluded that peak (*b*) occured *below* (not at) the phase transition temperature from the higher temperature solid to $S^*_{C_A}$, because they observed crystalline patterns of the Raman spectra in the temperature range between peaks (*b*) and (*d*). However, it is reasonable that the crystalline patterns were observed in the temperature range, because the stabilization to a more stable crystalline state occurs at the exothermic peak (*c*) immediately following peak (*b*). We also reported crystalline patterns of X-ray diffraction in the same temperature range [5]. In addition, an endothermic peak (entropy increase such as chain melting) should be associated to any change of the gradient of the Gibbs energy (G), because of a general relation $(\partial \Delta G/\partial T)_p = -\Delta S$. Thus, their microscopic interpretation that peak (*b*) is due to partial chain melting and our macroscopic interpretation that the change corresponds to the higher temperature solid to the $S^*_{C_A}$ phase transition are compatible.

[16] YVON, K., JEITSCHKO, W., and PARTHE, E., 1977, PULVERIX, Laboratoire de Crystallographie aux Rayons X, University of Geneva.